Quantitative Flow Visualization: Toward a Comprehensive Flow Diagnostic Tool[1]

MORY GHARIB,[2] FRANCISCO PEREIRA, DANA DABIRI, JAY R. HOVE, AND DARIUS MODARRESS

Graduate Aeronautical Laboratory, California Institute of Technology, Pasadena, California

SYNOPSIS.   Quantitative flow visualization has many roots and has taken several approaches. The advent of digital image processing has made it possible to practically extract useful information from every kind of flow image. In a direct approach, the image intensity or color (wavelength or frequency) can be used as an indication of concentration, density and temperature fields or gradients of these scalar fields in the flow (Merzkirch, 1987). For whole-field velocity measurement, the method of choice by experimental fluid mechanicians has been the technique of *Particle Image Velocimetry* (*DPIV*). This paper presents a novel approach to extend the DPIV technique from a planar method to a full three-dimensional volume mapping technique useful in both engineering and biological applications.

INTRODUCTION

In general, the optical flow or the motion of intensity fields can be obtained through time sequenced images (Singh, 1991). For example, the motion of patterns generated by dye clouds or particles can be used to obtain such a time sequence. The main problem with using a continuous-intensity pattern, generated by scalar fields (*e.g.*, dye patterns), is that it must be fully resolved (space/time) and contain variations of intensity at all scales before mean and turbulent velocity information can be obtained (Pearlstein and Carpenter, 1995). In this respect, the discrete nature of images generated by seeding particles has made particle tracking the method of choice for whole field velocimetry. Various methods such as individual tracking of particles or statistical techniques can be used to obtain the displacement information and subsequently the velocity information. The spatial resolution of this method depends on the number density of the particles.

The particle image velocimetry (PIV) technique follows a group of particles through statistical correlation of sampled windows of the image field (Adrian, 1991). This scheme removes the problem of identifying individual particles, which is often associated with tedious operations and large errors in the detection of particle pairs. In terms of the spatial resolution, the obtained velocity at each window represents the average velocity of the group of particles within the window. The interrogating window in PIV is the equivalent of the grid cell in CFD. Development of the video-based digital version of PIV, known as DPIV (Willert and Gharib, 1991; Westerweel, 1993), resulted directly from advances in charge coupled device (CCD) technology and fast, computer-based, image processing systems.

The capability of *whole field measurement* techniques in providing velocity vector or scalar field information in a format compatible to CFD calculations has made a major impact in defining common grounds for designing new approaches toward resolving the turbulent and two-phase flow problem. Such common grounds are difficult or impossible to define by using methods such as LDV or hot wire anemometry that do not address the global Lagrangian or the temporal nature of complex flows.

DPIV can be utilized to obtain three components of the velocity field. However, this extension of DPIV is limited to a few planes and cannot address the full dimensionality of turbulent flows with the current video technology. *Holographic PIV techniques* are more suitable for obtaining three-dimensional (3D) distribution of the velocity vector field (Barnhart *et al.*, 1994). The photographic nature of holographic PIV techniques limits their ability to address the temporal dynamics of turbulent flows. Recent advances in 3D video-based particle tracking techniques have removed some of these shortcomings (Kasagi and Sata, 1992). However, complexities involved in the optics, calibration and image processing of multiple-cameras and images severely limit wide-range application of multiple-camera stereo techniques.

An emerging technology that has a good potential for resolving difficulties associated with aforementioned flow mapping techniques is the *method of defocusing imaging* (Willert and Gharib, 1992). *Defocusing Digital Particle Image Velocimetry* (*DDPIV*) is the natural extension of planar PIV techniques to the third spatial dimension. This method has shown great potential for two-phase flow studies (Pereira *et al.*, 2000; Pereira and Gharib, 2002).

THE DEFOCUSING CONCEPT

Willert and Gharib (1992) established the foundations of the defocusing concept for flow visualization. We report here the most important aspects in a revised form. For clarity, we will use the term *particle* when referring to both a solid particle and to a bubble.

A typical 2D imaging system, consisting of a converging lens and of an aperture, is represented in Figure 1 to help describe the DDPIV technique. Figure
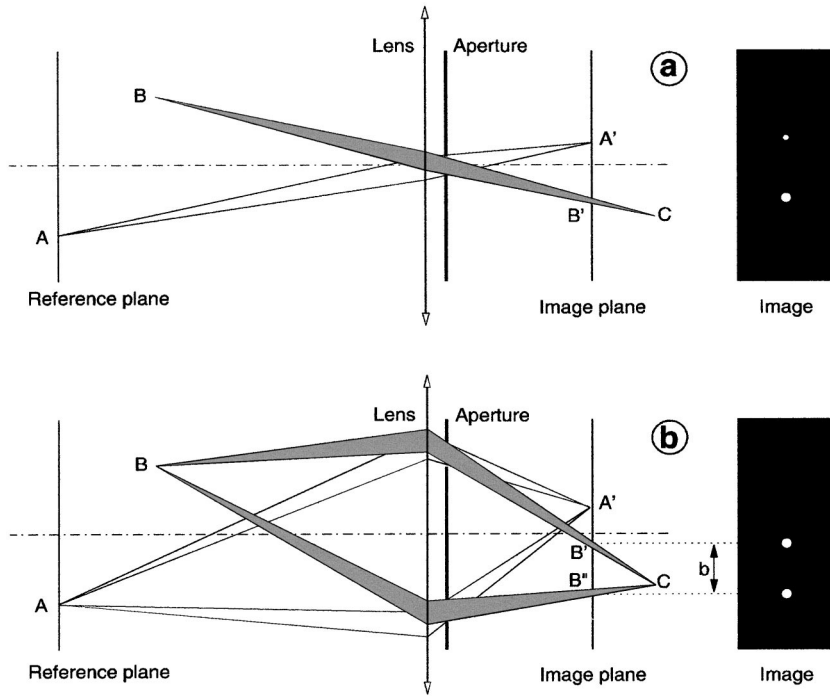
FIG. 1. a) Standard 2D imaging system increases depth of field by utilizing a small aperature (large f-stop). Utilizing an off-axis shift of the aperture a proportional shift on the sensor plane can be accomplished for defocused objects. B) A two aperture design generates two images of the defocused object. See text for detailed explanation.

1a exhibits a point *A*, located on the object plane (or reference plane), and a point *B* placed in between this plane and the lens system. Point *A* appears focused in *A'*, on the image plane (or sensor plane), while *B* is projected as a blurred image *B'* coming into focus beyond the image plane at *C*. The DDPIV technique (Fig. 1b) uses a mask with two or more apertures shifted away from the optical axis to obtain multiple images (*B'* and *B''*) from each scattering source. The image shift b on the image plane, caused by these off-axis apertures, is related to the depth location of the source points, whereas the scattered light intensity combined with the blurredness is used to recover the size information.

Geometric Analysis

A simplified geometric model of a two-aperture defocusing optical arrangement is represented in Figure 2. The interrogation domain is defined as a cube of side *a*, thus a square in the plane. The back face of this cube is on the reference plane, which is placed at a distance *L* from the lens plane. Let *d* be the distance between apertures, *f* the focal length of the converging lens and *l* the distance from the lens to the image plane. A pho-
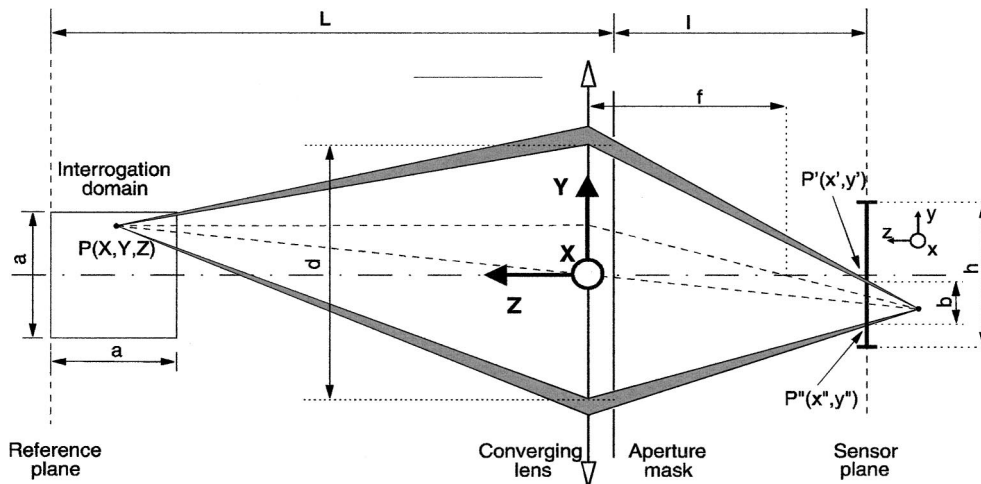

FIG. 2. A simplified geometric model of the two-aperture defocusing arrangement. See text for detailed explanation.
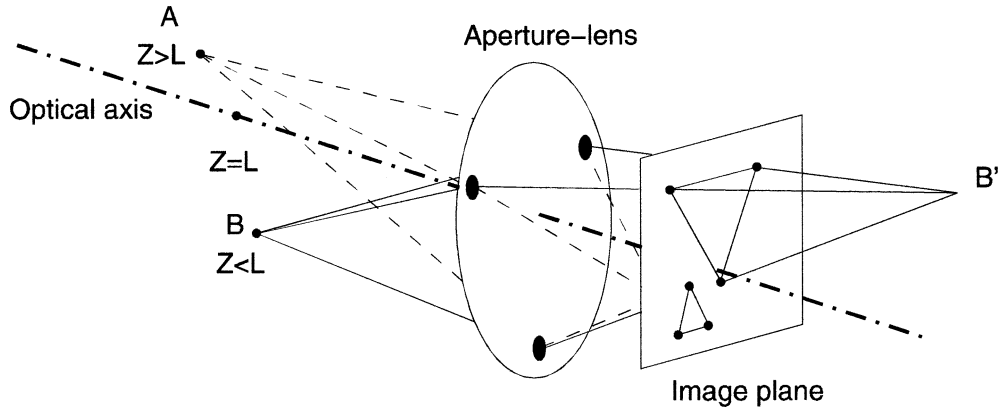
FIG. 3. A three-aperture defocusing arrangement. The orientation of the equilateral triangle resulting from this triple aperture mask indicates the relative position of the source with respect to the reference plane.

tosensor (*e.g.*, CCD), of height h, materializes the image plane. The physical space is mapped to a coordinate system originating in the lens plane, with the Z-axis on the optical axis of the system. Coordinates in the physical space are designated (X,Y,Z). The image coordinate system is simply the Z-translation of the physical system onto the sensor plane, *i.e.,* at $Z = -l$. The coordinates of a pixel on the imaging sensor are given by the pair (x,y). Point $P(X,Y,Z)$ represents a light scattering source such as particle, bubble, point-like dot, etc. For $Z \neq L$, P is projected onto points $P'(x', y')$ and $P''(x'',y'')$, separated by the distance b.

The coordinates (x', y') and (x'', y'') of the images

P' and P'' of $P(X,Y,Z)$ in the image plane are given by the following relations:

$$x' = x'' = -ML\frac{X}{Z}$$

$$y' = \frac{M}{2Z}[d(L - Z) - 2LY]$$

$$y'' = \frac{M}{2Z}[-d(L - Z) - 2LY] \qquad (1)$$

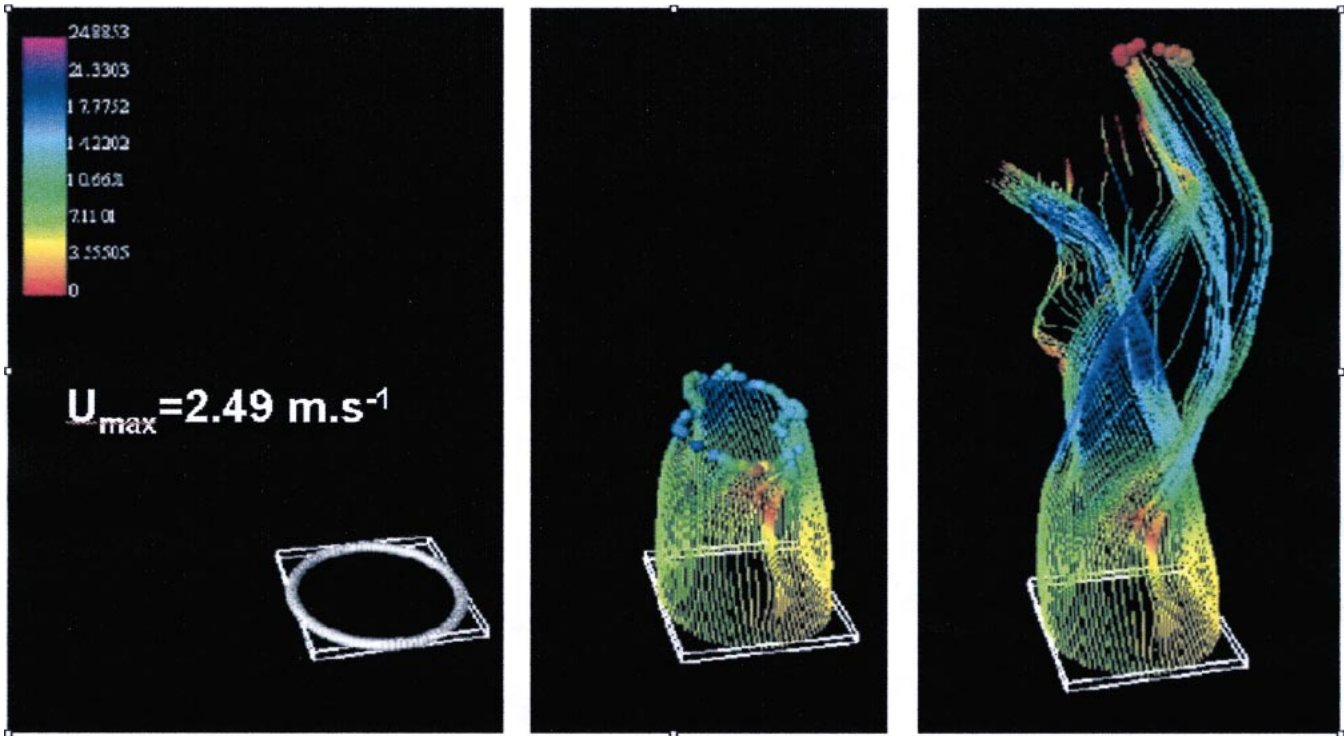Where M is the optical magnification provided by the lens equation.

FIG. 4. Mapping complex flow. Pathlines of air bubbles passing through a propellor spinning at 12 rps. Bubbles trapped in the vortical flow induced by the propellor reach a maximum velocity of 2.49 m sec^{-1} in the outer region of the propellor. Color scale indicates velocity m sec^{-1}.
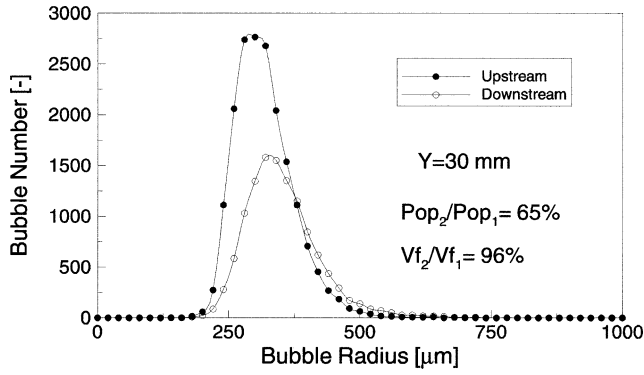
FIG. 5. Size distribution of air bubbles passing through a propellor spinning at 12 rps. A histogram of bubble size both upstream and downstream of the propellor from a population of approximately 10,000. The ratio of the upstream to downstream population is 65% but the ratio of the respective void fractions is close to 100%. The propellor is located on the Y vertical axis of the flow at Y ≈ 30 mm.

The image separation vector *b* represents the distance between the images *P'* and *P''*. The norm is therefore given by:

$$b = \frac{Md}{Z}(L - Z)$$

$$= \frac{1}{K}\left(\frac{1}{Z} - \frac{1}{L}\right) \quad \text{with } K = \frac{1}{MdL} \tag{2}$$

Eq. 2 demonstrates the extreme simplicity of the defocusing concept, which, of course, is greatly valuable in terms of computational implementation and processing speed. In purely geometric terms, the image separation *b* is independent of the in-plane coordinates *X* and *Y*. Likewise, the pinhole diameter has no bearing on *b* and is only responsible for the amount of blurredness of any given particle image. For our prototype instrument, we use three pinholes, arranged into a triangular pattern. This configuration, shown in Figure 3,
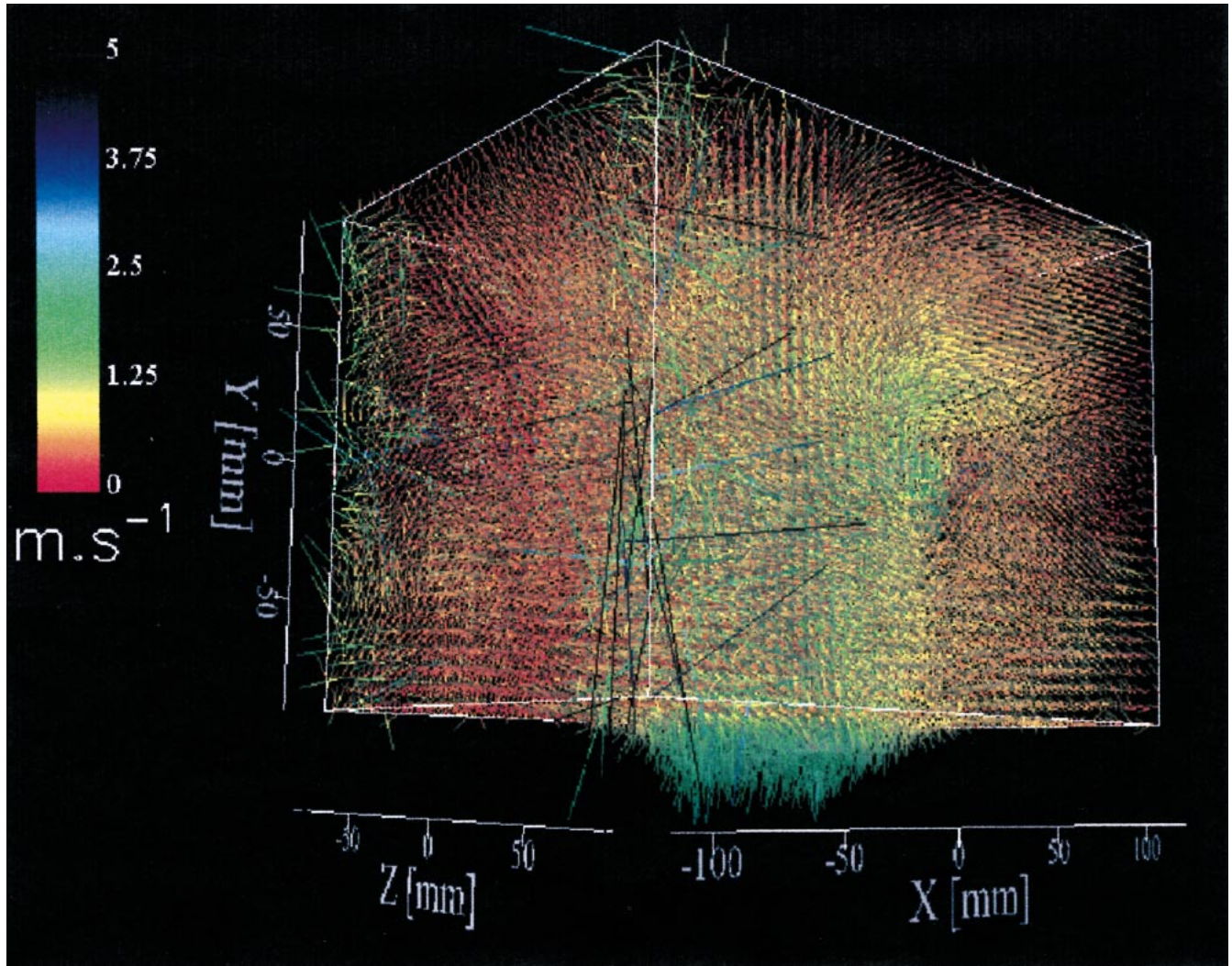

FIG. 6. Velocity field generated by a 3-blade boat propeller rotating at 12 Hz represented as the phase-average of 50 instantaneous velocity fields. Image represents a volume of dimensions $200 \times 200 \times 400$ mm³ and contains 72,963 vectors (33*33*67 voxels). Color scale indicates velocity m sec⁻¹.
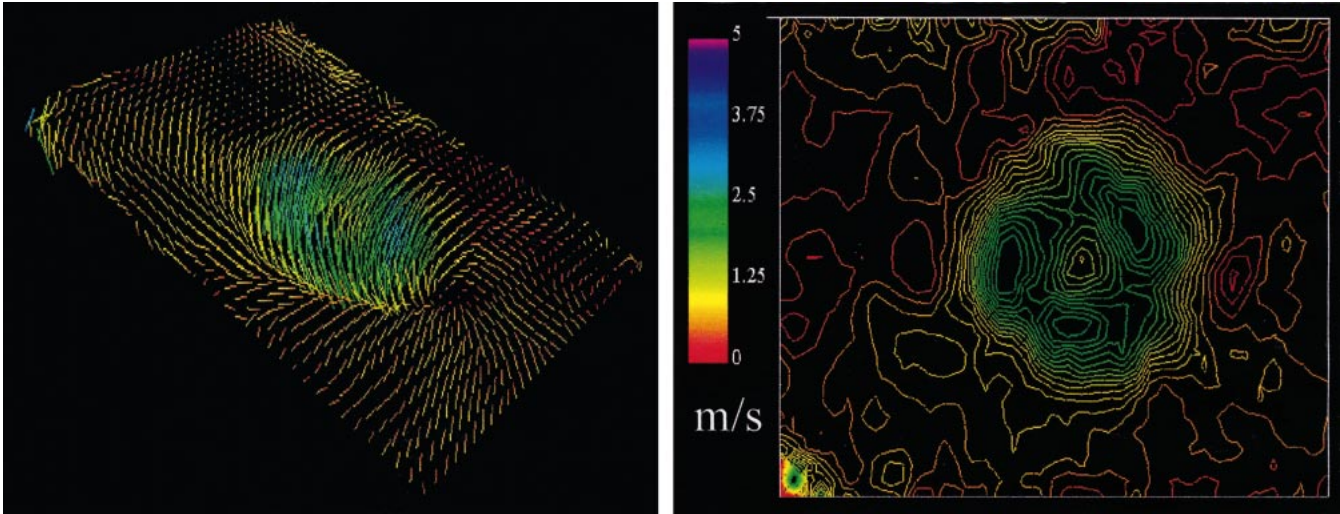
Fig. 7. Left: velocity cross-section (downstream region, 0.5 diameter) from 3-blade propeller volume depicted in Figure 6. Note the high-speed jet core along the downstream section of the propeller axis. Right: corresponding isovelocity contour revealing a viscous wake rapidly fading into the bulk flow. Color scale indicates velocity m sec⁻¹.

exhibits a flipping triangle when P moves across the reference plane and requires straightforward and fast image processing routines.

The sensitivity of the system (*i.e.*, its ability to detect small changes of the particle location) can be evaluated through the separation gradient:

$$\frac{\partial b}{\partial Z} = -\frac{1}{KZ^2} \tag{3}$$

The coordinates of P in the world coordinate system are derived from the image coordinates of the projections P' and P'' (see Eq. 1) as:

$$X = -\frac{x_0 Z}{ML} \quad \text{with } x_0 = \frac{x' + x''}{2}$$

$$Y = -\frac{y_0 Z}{ML} \quad \text{with } y_0 = \frac{y' + y''}{2}$$

$$Z = \frac{1}{\frac{1}{L} + Kb} \tag{4}$$

Assuming that the apertures are equidistant from the origin of the coordinate system, the image point defined by (x_0, y_0) is the image of the particle if there were a single aperture at the origin.

A camera system has been designed and fabricated based upon the above concept (Pereira *et al.*, 2000). In this system the velocity vector field is obtained by local spatial cross-correlation between small volume elements (*voxels*) containing particles observed at two time steps.

APPLICATIONS

To date we have tested our system on flow patterns generated by two- and three-blade propellers and, most recently, on volumetric mapping of the body of swimming boxfishes (*Ostracion meleagris*).

Case 1: A two-blade model propeller is immersed into a water tank and rotates at 12 rps, corresponding to a tangential velocity of 2.52 m sec⁻¹ at the tip of the blades. A bubble generator is placed below the propeller, producing a dense stream of rising sub-millimeter air bubbles. A velocity field of the rising bubbles is obtained through phase averaging images.

A 3-D velocity field is obtained after averaging and outlier correction. Mass-less particles are then artificially injected into the mean velocity data set, in a radial arrangement and one diameter upstream the propeller. Paths of bubbles are determined, providing a unique insight into this complex flow as shown in Figure 4. Color level relates to the local measured velocity amplitude. Velocity reaches a maximum of 2.49 m sec⁻¹ in the outer region of the propeller, matching closely the blade tip tangential velocity.

The bubble mean radius along the Y vertical axis of the flow (rotation axis of the propeller) is reported in Figure 5. The mean radius increases almost linearly to nearly 325 μm at $Y \approx 30$ mm, where the propeller is located. After the bubbles leave the immediate vicinity of the propeller, their radius decreases decreasing to about 200 μm. The growth of bubbles is partly due, but to a very small extent, to the decrease of the static pressure with increasing Y. In fact, bubbles initially experience low pressure on the suction side of the propeller before passing into the high-pressure region where they collapse.

Included in Figure 5 are the histograms calculated taking the same volume below and above $Y = 30$ mm. The histogram peak follows the trend outlined before due to the pressure variations. The ratio of the upstream to the downstream populations is 65%. However, the ratio of the respective void fraction is close
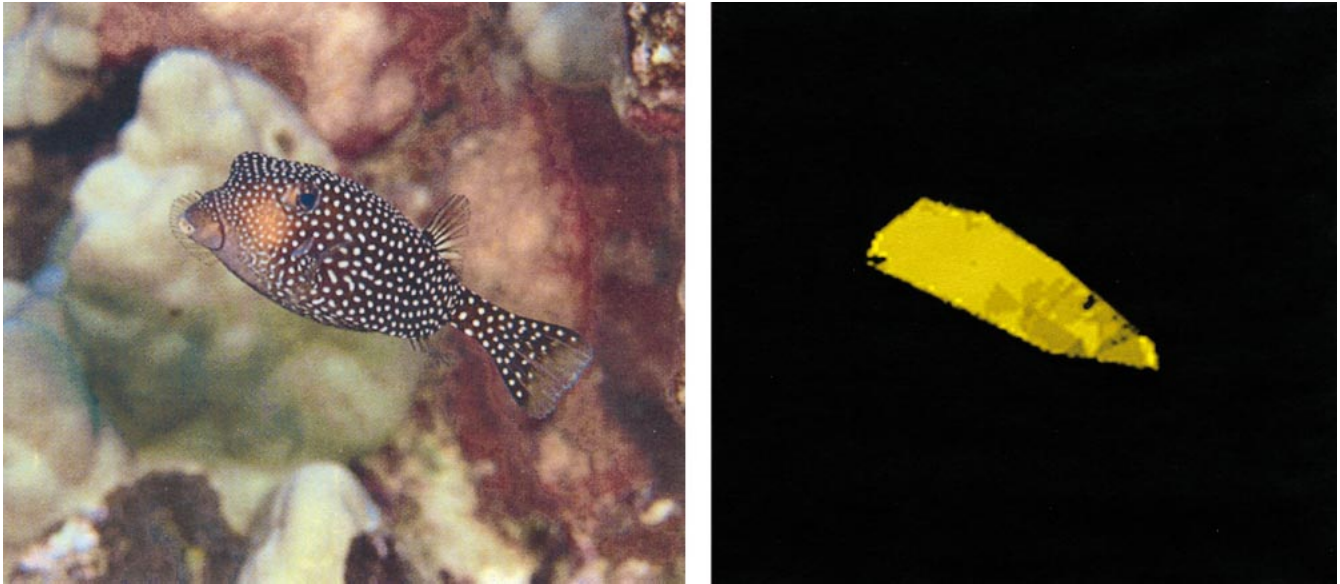
FIG. 8. Left: Free swimming spotted boxfish (*Ostracion meleagris*). Right: Volumetric map of boxfish carapace from fish swimming in an aquarium.

to 100%. These observations indicate that coalescence of bubbles is the main mechanism acting here, although breakup may occur in the propeller region.

Case 2: *A three-blade boat propeller* of similar configuration to that described above is rotated at 12 Hz. The velocity field represented in Figure 6 is obtained by phase-averaging a sequence of 50 instantaneous velocity fields. Spurious vectors can be seen on borders of the interrogation domain. A slice in the velocity field (Fig. 7, left panel) clearly displays the high-speed jet core along the downstream section of the propeller axis. However, the isovelocity contours (Fig. 7, right panel) show a viscous wake that appears as a velocity defect due to the merging of the two boundary layers from the blades. A slight contraction of the slipstream could also be detected. The wake is found to rapidly fade into the bulk flow.

Case 3: *Living boxfishes* represent an ideal natural analog to man-made autonomous underwater vehicles (AUVs) with their rigid carapace and equally spaced peripheral control surfaces (fins) (Hove *et al.*, 2002). The bony carapace of these animals has been shown to contribute to their dynamic stability (Bartol *et al.*, 2002). Using the naturally occurring, smallish, white spots on the fish's body as the "particles" defining the three-dimensional body space, we created a volumetric map of the boxfish carapace as the animal swam in an aquarium. The resulting reconstruction (Fig. 8) shows great promise for reconstructing moving volumes regardless of their geometric complexity.

SUMMARY

In this paper we seek to present some recent advances in the field of quantitative flow visualization and demonstrate their utility in better understanding both synthetic and biological flows. Only techniques that can provide time resolved, three-dimensional velocity vector fields will be on common ground with CFD. In this respect the novel method of DDPIV described here has the potential to provide quantitative flow information comparable with that of CFD.

REFERENCES

Adrian, R. J. 1991. Particle-imaging techniques for experimental fluid mechanics. Annual Rev. Fluid Mech. 23:261–304.

Barnhart, D. H., R. J. Adrian, and G. C. Papen. 1994. Phase-conjugate holographic system for high resolution PIV. Appl. Optics 3(30):7159–7170.

Bartol, I. K., M. Gharib, D. Weihs, P. W. Webb, J. R. Hove, and M. S. Gordon. 2002. Dynamic stability of swimming in ostraciid fishes: Role of the carapace in the smooth trunkfish *Lactophrys triqueter* (Teleostei: Ostraciidae). J Exp. Biol. (In press).

Hove, J. R., L. M. O'Bryan, M. S. Gordon, P. W. Webb, and D. Weihs. 2002. Boxfishes (Teleostei: Ostraciidae) as a model system for fishes swimming with many fins: Kinematics. J. Exp. Biol. 204:1459–1471.

Kasagi, N. and Y. Sata. 1992. Recent development in three-dimensional particle tracking velocimetry. Proceedings of Flow Visualization Conference VI, Yokohama, Japan.

Merzkirch, W. 1987. *Flow visualization.* 2nd ed. Academic Press, Orlando, Florida.

Pearlstein, A. J. and B. Carpenter. 1995. On the determination of solenoidal or compressible velocity fields from measurements of passive and reactive scalars. Physics of Fluids 7(4):754–763.

Pereira, F. and M. Gharib. 2002. Defocusing digital particle image velocimetry and the three-dimensional characterization of two-phase flows. Meas. Sci. Technol. 13:683–694.

Pereira, F., M. Gharib, M. Modarress, and D. Dabiri. 2000. Defocusing DPIV: A 3-component 3-D DPIV measurement technique, application to bubbly flows. Experiments in Fluids 29: S78–S84.

Singh, A. 1991. Optic flow computation. Computer Society Press, IEEE.

Westerweel, J. 1993. Digital image velocimetry: Theory and application. Ph.D. Thesis, Delft University Press, Delf.

Willert, C. E. and M. Gharib. 1991. Digital particle image velocimetry. Experiments in Fluids 10:181–193.

Willert, C. E. and M. Gharib. 1992. Three-dimensional particle imaging with a single camera. Experiments in Fluids 12:353–358.